

Article

Pt-Sn Supported on Beta Zeolite with Enhanced Activity and Stability for Propane Dehydrogenation

Su-Un Lee, You-Jin Lee, Soo-Jin Kwon, Jeong-Rang Kim *  and Soon-Yong Jeong

Chemical & Process Technology Division, Korea Research Institute of Chemical Technology, 141, Gajeong-ro, Yuseong-gu, Daejeon 34114, Korea; sulee@kRICT.re.kr (S.-U.L.); eugene@kRICT.re.kr (Y.-J.L.); soosoo24@naver.com (S.-J.K.); syjeong@kRICT.re.kr (S.-Y.J.)

* Correspondence: jrkim@kRICT.re.kr; Tel.: +82-4-860-7324

Abstract: With the growing global propylene demand, propane dehydrogenation (PDH) has attracted great attention for on-purpose propylene production. However, its industrial application is limited because catalysts suffer from rapid deactivation due to coke deposition and metal catalyst sintering. To enhance metal catalyst dispersion and coke resistance, Pt-based catalysts have been widely investigated with various porous supports. In particular, zeolite can benefit from large surface area and acid sites, which favors high metal dispersion and promoting catalytic activity. In this work, we investigated the PDH catalytic properties of Beta zeolites as a support for Pt-Sn based catalysts. In comparison with Pt-Sn supported over θ -Al₂O₃ and amorphous silica (Q6), Beta zeolite-supported Pt-Sn catalysts exhibited a different reaction trend, achieving the best propylene selectivity after a proper period of reaction time. The different PDH catalytic behavior over Beta zeolite-supported Pt-Sn catalysts has been attributed to their physicochemical properties and reaction mechanism. Although Pt-Sn catalyst supported over Beta zeolite with low acidity showed low Pt dispersion, it formed a relatively lower amount of coke on PDH reaction and maintained a high surface area and active Pt surfaces, resulting in enhanced stability for PDH reaction. This work can provide a better understanding of zeolite-supported Pt-Sn catalysts to improve PDH catalytic activity with high selectivity and low coke formation.



Citation: Lee, S.-U.; Lee, Y.-J.; Kwon, S.-J.; Kim, J.-R.; Jeong, S.-Y. Pt-Sn Supported on Beta Zeolite with Enhanced Activity and Stability for Propane Dehydrogenation. *Catalysts* **2021**, *11*, 25. <https://doi.org/10.3390/catal11010025>

Received: 30 November 2020

Accepted: 22 December 2020

Published: 28 December 2020

Publisher's Note: MDPI stays neutral with regard to jurisdictional claims in published maps and institutional affiliations.



Copyright: © 2020 by the authors. Licensee MDPI, Basel, Switzerland. This article is an open access article distributed under the terms and conditions of the Creative Commons Attribution (CC BY) license (<https://creativecommons.org/licenses/by/4.0/>).

Keywords: propylene; propane dehydrogenation; zeolite; Beta; Pt; Sn

1. Introduction

Propylene is an indispensable building block for producing a variety of important monomers, polymers, and intermediates, such as polypropylene, propylene oxide, acrylonitrile, acrylic acid, and so forth [1]. The global propylene demand is expected to grow by 35% to 135 million tons in 2025, compared with 100 million tons in 2017 [2,3]. Conventional processes, such as naphtha steam cracking and fluid catalytic cracking, which produce propylene as a by-product, will not satisfy the increasing propylene demand. Steam cracking and fluid catalytic cracking produced about 48% and 25% of propylene, respectively, but there is still the remaining propylene demand [4]. To make up for the deficient propylene supply, propane dehydrogenation (PDH) has attracted great attention for on-purpose propylene production because of its high propylene selectivity. Pt-based catalysts are known as the most active materials for catalyzing PDH, but their application is limited because coke deposition and metal sintering cause their rapid deactivation. Thus, doping promoters have been suggested to modify the electron density of Pt and weaken the adsorption of the product alkene, ultimately reducing undesirable side reactions such as cracking and coke deposition [5]. Among various promoters (e.g., In, Ga, Mn, Cu, and Zn), Sn has shown a remarkable suppression effect on rapid deactivation. Despite the improved catalytic behavior of Sn-promoted Pt-based catalysts, it still remains a daunting challenge to satisfy the industrial requirement for the deficient propylene supply because high con-

version could be achieved at high temperature, but undesired side reactions decrease the selectivity of propylene and stability of catalysts [6].

For a further practical improvement, Pt catalysts have been widely investigated with various supports, including Al_2O_3 , SiO_2 , SBA-15, L-zeolite, Y-zeolite, Beta, ZSM-5, and MOR. In particular, zeolites, aluminosilicates with pores of molecular dimensions, are interesting supports for PDH catalysts because they offer a large surface area favoring high metal dispersion. The three-dimensional pore structure of zeolites provides a potentially useful approach to impose the shape selectivity for inhibiting the side reaction [7,8] and promote the diffusion of mass [8–10]; thus, zeolites can enhance coke resistance and alleviate rapid deactivation. Moreover, zeolites possess Brønsted and Lewis acid sites, which are created by the substitution of Si^{4+} with Al^{3+} , on the negatively charged zeolite framework. These acid sites can strengthen the metal-support interaction and promote metal dispersion by strongly anchoring metal ions, reinforcing anti-sintering capability. In terms of catalytic activity, Lewis acid sites enhance the adsorption of reactants and increase the conversion of reaction, but do not activate alkanes to significantly change the selectivity of reaction [11]. On the other hand, Brønsted acid sites can promote cracking, oligomerization, and aromatization, resulting in coke formation [12,13]. In the literature, Pt-containing zeolites without Brønsted acid sites or weak acidity have been prepared by ion exchange and controlling the Si/Al ratio, and it has been confirmed that this enhanced PDH catalytic performance. Nevertheless, the zeolite-supported Pt-Sn catalysts have been mainly focused on the confinement effect within zeolite framework in aim to resolve the sintering of Pt [8,14–16].

In this work, we systematically investigated the PDH catalytic properties of Beta zeolite as a model zeolite support in Pt-Sn based catalysts because of its well-known framework with three-dimensional 12-ring pore structures, which are favorable for coke resistance. Beta zeolite-supported Pt-Sn catalysts with different acidity were prepared using Beta zeolites with $\text{SiO}_2/\text{Al}_2\text{O}_3$ ratio of 38 and 300, and their catalytic performance and stability for PDH were tested in a fixed-bed reaction system. To clarify the effect of the Beta zeolite-supported Pt-Sn catalysts on PDH regarding their acidity, the Pt-Sn catalysts supported over $\theta\text{-Al}_2\text{O}_3$ with Lewis acidity and amorphous silica (Q6) without acidity were prepared for comparison. In particular, the comparison with $\theta\text{-Al}_2\text{O}_3$ was conducted to assess the feasibility of industrial use because it is regarded as one of the best catalysts with high metal dispersion and it is commonly used in commercial PDH processes [17]. The supported Pt-Sn catalysts with various supports were thoroughly characterized by measurements of N_2 -physisorption, NH_3 -TPD, FT-IR of adsorbed pyridine, TEM, CO-chemisorption, XRD, and H_2 -TPR. Ultimately, the different PDH catalytic behavior over Beta zeolite-supported Pt-Sn catalysts can be attributed to their physicochemical properties and reaction mechanism.

2. Results and Discussion

2.1. Physicochemical Properties of the Supported Pt-Sn Catalysts

The N_2 adsorption–desorption isotherms in Figure 1 demonstrate the structural characteristics of Beta zeolites, $\theta\text{-Al}_2\text{O}_3$, Q6, and the supported Pt-Sn catalysts. Table 1 summarizes the surface area and pore volume, calculated from the N_2 adsorption–desorption isotherms. Beta zeolites belong to a three dimensional 12-ring pore system with channels of 6.5×5.6 and 7.5×5.7 Å diameters for two channel types of *BEA (Zeolite Beta polymorph A). The type I isotherms of Beta(300) and Beta(38) show high nitrogen uptakes at low relative pressures and a well-defined plateau, indicating the typical characteristic of microporous materials. Regardless of the $\text{SiO}_2/\text{Al}_2\text{O}_3$ ratio, Beta(300) and Beta(38) possess similar surface areas and pore volumes. The isotherms of $\theta\text{-Al}_2\text{O}_3$ and Q6 show the typical type IV adsorption–desorption isotherm with a hysteresis loop at high relative pressure, indicating the presence of mesopores or interparticular space. However, uptakes at low relative pressure in the isotherms of $\theta\text{-Al}_2\text{O}_3$ and Q6 are much lower than that of Beta zeolites, and they represent smaller BET surface area and pore volume in the microporous

range. After Sn and Pt were loaded by sequential wet impregnation, all the supported Pt-Sn catalysts preserved the BET specific surface area and pore volume of the pristine support with a slight decrease due to a small loading amounts of Pt (0.82 wt%) and Sn (0.22 wt%).

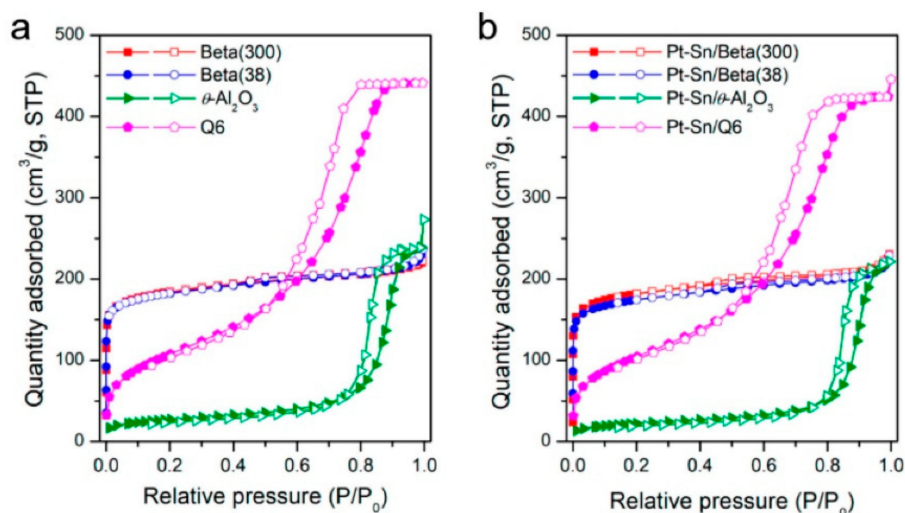


Figure 1. N₂ adsorption–desorption isotherms of (a) supports and (b) supported Pt-Sn catalysts.

Table 1. Porous properties of supports and supported Pt-Sn catalysts obtained by N₂ adsorption–desorption isotherm.

Sample	Surface Area (BET) (m ² /g)			Pore Volume (cm ³ /g)		
	Total ^a	Micropore ^b	Mesopore ^b	Total	Micropore ^b	Mesopore ^b
Beta(300)	705	540	165	0.32	0.21	0.11
Beta(38)	696	523	173	0.36	0.21	0.15
θ-Al ₂ O ₃	96	21	76	0.43	0.01	0.42
Q6	391	4	387	0.69	-	0.69
Pt-Sn/Beta(300)	694	531	163	0.34	0.21	0.13
Pt-Sn/Beta(38)	665	511	154	0.34	0.20	0.14
Pt-Sn/θ-Al ₂ O ₃	80	14	66	0.35	0.01	0.34
Pt-Sn/Q6	386	1	385	0.67	-	0.67

^a Total surface area was determined by N₂ adsorption and calculated by BET method. ^b Surface area and volume of micropore and mesopore were determined by t-plot method.

The acidic properties of the prepared samples were examined by NH₃-TPD profiles in Figure 2, and the concentration of their acid sites were estimated as shown in Table 2. The NH₃-TPD profiles of the Beta zeolite-supported Pt-Sn catalysts showed the typical two NH₃ desorption peaks at approximately 185 °C (weak acid sites) and 310 °C (strong acid sites). Due to the fact that the Al content in zeolite creates acid sites by raising the electronic imbalance on the neutral silica framework, it is obvious that the number of acid sites in Beta(38) is 4.6 times higher than that in Beta(300). In the case of Pt-Sn/θ-Al₂O₃ as the alumina-supported Pt-Sn catalyst, the number of its acid sites is between that of the Pt-Sn/Beta(38) and Pt-Sn/Beta(300) catalysts with a similar acid strength distribution. As the silica-supported Pt-Sn catalyst, Pt-Sn/Q6 shows the absent acidic property. It was reported that the conversion and selectivity for PDH are strongly related to not only the number of acid sites, but also the types of acid sites [12]. For example, Brønsted acid sites are active in oligomerization and cyclization for alkane aromatization, or Brønsted acid sites coupled with Lewis acid sites can effectively enhance catalytic reactions [12]. Therefore, the types of acid sites were distinguished as Brønsted (B) or Lewis (L) acid sites by measuring the FT-IR spectra of adsorbed pyridine, as shown in Figure 3, and the ratio of B/L acid sites is summarized in Table 2. The Pt-Sn/Beta(300) and Pt-Sn/Beta(38) catalysts contain Brønsted acid sites and Lewis acid sites with B/L ratios of 1.22 and 1.07, respectively, but

the Pt-Sn/ θ -Al₂O₃ catalyst has only Lewis acid sites. Specifically, the numbers of Brønsted and Lewis acid sites were calculated by multiplying the total acid site concentration from NH₃-TPD and the B/L ratio from FT-IR measurement. The Pt-Sn/Beta(38) catalyst contains similar number of Lewis acid sites as that of the Pt-Sn/ θ -Al₂O₃ catalyst, but it also has the same number of Brønsted acid sites as Lewis acid sites.

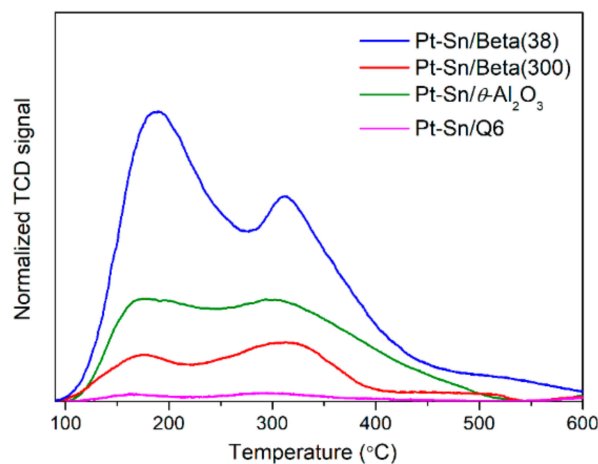


Figure 2. NH₃-TPD profiles of supported Pt-Sn catalysts.

Table 2. Acidic properties of supported Pt-Sn catalysts from NH₃-TPD and FT-IR after pyridine adsorption.

Sample	NH ₃ -TPD (mmol/g)			FT-IR after Pyridine Adsorption	Calculation(mmol/g)	
	Weak Acid Site (100–250 °C)	Strong Acid Site (250–500 °C)	Total	B/L	B	L
Pt-Sn/Beta(300)	0.07	0.10	0.17	1.22	0.09	0.08
Pt-Sn/Beta(38)	0.39	0.39	0.78	1.07	0.40	0.38
Pt-Sn/ θ -Al ₂ O ₃	0.15	0.21	0.36	0	0	0.36
Pt-Sn/Q6	0.01	0.01	0.02	-		

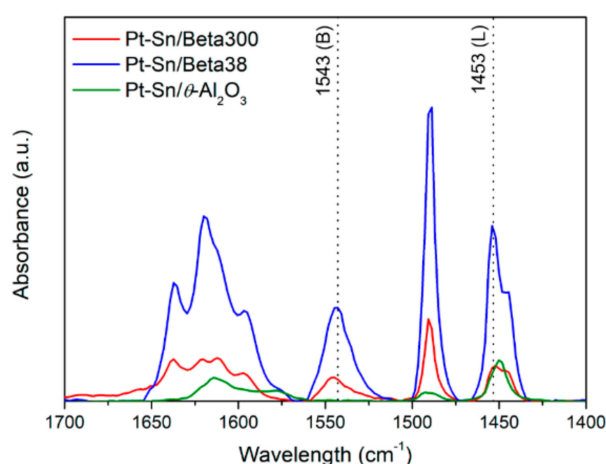


Figure 3. FT-IR spectra of adsorbed pyridine over supported Pt-Sn catalysts.

The morphology and distribution of Pt and Sn in the supported Pt-Sn catalysts were observed by transmission electron microscopy (TEM), as shown in Figure 4. Generally, due to larger atomic numbers of metals, metal elements on TEM images are distinctive with darker color than zeolite. In particular, Pt-Sn/Beta(300) and Pt-Sn/Q6 showed the formation of nanoparticles with dark color, which should be the wet-impregnated Pt-

Sn catalysts. Compared to Pt-Sn/Beta(300) with a similar surface area (Figure 4a), Pt-Sn/Beta(38) showed very well-dispersed nanoparticles without distinct aggregation of particles (Figure 4b). This can be attributed to the acidic surface of Beta zeolites with a low SiO₂/Al₂O₃ ratio, which can strengthen the interaction with the Pt-Sn species and lead to high dispersion of the supported metal species. In the same manner, it is obvious that the Pt-Sn/ θ -Al₂O₃ catalyst exhibits good distribution of the Pt-Sn species without agglomeration over the acidic surface of the θ -Al₂O₃ support (Figure 4c) and Pt-Sn/Q6 shows the supported metal species in tens of nanometers due to the neutral surface of the silica support (Figure 4d). The Pt dispersion of each catalyst was quantized by CO-chemisorption, as shown in Table 3, and the same trend was also observed on the order of Pt-Sn/Q6 (1.7%) < Pt-Sn/Beta(300) (12.2%) < Pt-Sn/Beta(38) (61.6%) < Pt-Sn/ θ -Al₂O₃ (82.8%). Pt-Sn/ θ -Al₂O₃ achieves the highest dispersion despite its low surface area, and this may be due to the fact that the acidity of the supports is strongly related to Pt dispersion [18].

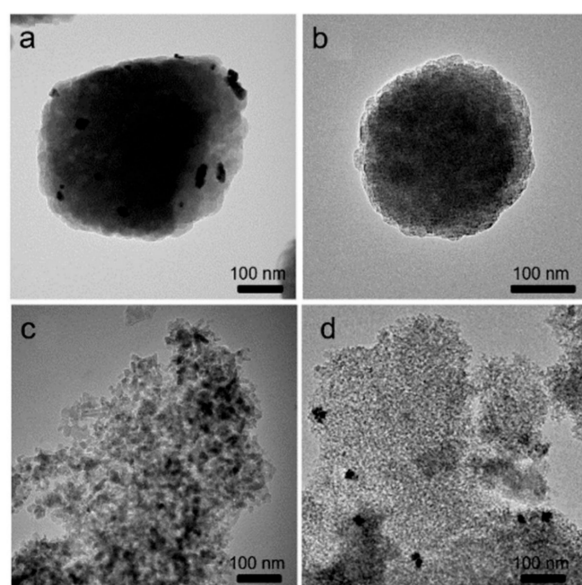


Figure 4. TEM images of supported Pt-Sn catalysts: (a) Pt-Sn/Beta(300), (b) Pt-Sn/Beta(38), (c) Pt-Sn/ θ -Al₂O₃, and (d) Pt-Sn/Q6.

Table 3. Pt-dispersion of supported Pt-Sn catalysts estimated by CO chemisorption.

Catalyst	Pt Dispersion (%)
Pt-Sn/Beta(300)	12.2
Pt-Sn/Beta(38)	61.6
Pt-Sn/ θ -Al ₂ O ₃	82.8
Pt-Sn/Q6	1.7

The XRD patterns in Figure 5 confirm the crystalline structure of Beta and θ -Al₂O₃ with their characteristic diffraction peaks, and the amorphous structure of Q6 with the absence of diffraction peaks. Regarding the Pt and Sn phase, the supported Pt-Sn catalysts exhibit peaks at 2θ of 39.7° and 46.2°, which correspond to the reflection of the (111) and (200) planes of Pt in a face-centered-cubic (fcc) structure. The formation of fcc Pt can result from the oxidative decomposition of H₂PtCl₆ used as a Pt precursor under calcination at 600 °C. According to the previously reported literature [19,20], the oxidative decomposition of H₂PtCl₆ is represented at different temperatures as follows:

- (1) H₂PtCl₆·6H₂O → PtCl₄ + 2HCl + 6H₂O [25–280 °C];
- (2) PtCl₄ → PtCl₂ + Cl₂ [280–350 °C];
- (3) PtCl₂ → Pt + Cl₂ [350–530 °C].

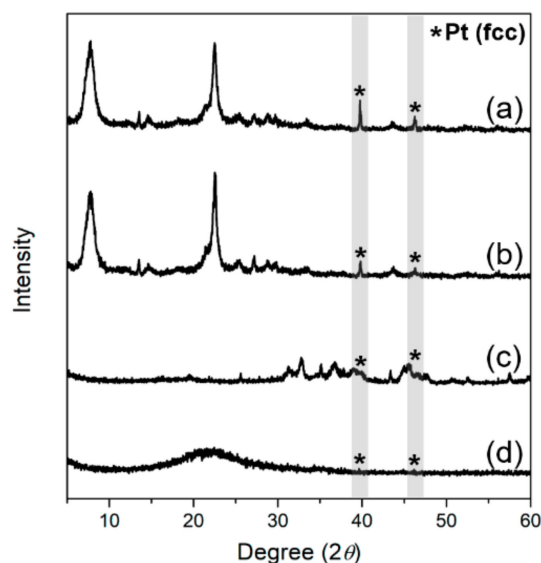


Figure 5. XRD patterns of supported Pt-Sn catalysts: (a) Pt-Sn/Beta(300), (b) Pt-Sn/Beta(38), (c) Pt-Sn/ θ -Al₂O₃, and (d) Pt-Sn/Q6.

On the other hand, the phases of Pt_xSn_{1-x} alloy and/or SnO_x were not detected in the XRD patterns, so we assumed that the Pt-Sn nanoparticles were formed in the fcc structure of metallic Pt crystals, as Sn atoms entered the cubic Pt lattice [21]. Pt-Sn/Beta(300) exhibits a higher intensity of Pt diffraction peaks than Pt-Sn/Beta(38). This indicates that particle size decreases with low SiO₂/Al₂O₃ ratio of Beta zeolites, which is in good agreement with the TEM results. Pt-Sn/ θ -Al₂O₃ do not show distinct XRD diffraction peaks due to overlapping with the θ -Al₂O₃ diffraction peaks, and small particle size was confirmed by the TEM results. However, it is intriguing that the XRD pattern of Pt-Sn/Q6 showed very low intensity although it has the lowest Pt dispersion. According to literature, the hydrophobic surface of silica in comparison to acidic supports makes it less favored for the adsorption of [PtCl₆]²⁻ and the formation of the proposed Pt complex. This aspect, in the case of Pt-Sn/Q6, may hamper the oxidative decomposition of H₂PtCl₆ and still preserve Pt(IV), such as the form of oxychloride PtO_xCl_y [22].

To further investigate the oxidation states of the metal species, the TPR profiles of the calcined catalysts were obtained, as shown in Figure 6. The H₂-TPR profiles of the Beta zeolite-supported Pt-Sn catalysts show an H₂-consumption peak with very low intensity, which can be attributed to the fact that the metallic Pt phase was already formed by the oxidative decomposition of Pt precursors during the calcination of catalyst preparation. On the other hand, Pt-Sn/Q6 shows a single peak at 125 °C that can be assigned to the reduction of Pt(IV) to Pt(0). Combining the XRD results showing the absence of metallic Pt phase, the H₂-consumption in Pt-Sn/Q6 indicates the existence of Pt species fully unreduced under the calcination condition. In the case of the Pt-Sn/ θ -Al₂O₃ catalyst, three reduction peaks were interestingly observed at 126, 240, and 389 °C. Like the case of the Pt-Sn/Q6, the reduction peak at 126 °C indicates the remaining unreduced Pt species. In addition, the peaks at 240 and 389 °C can be assigned to the co-reduction of Pt and Sn species and the reduction of SnO_x species, respectively [23]. Therefore, This may be one of the reasons for low intensity in the XRD pattern of Pt-Sn/ θ -Al₂O₃ among the supported Pt-Sn catalysts over acidic supports.

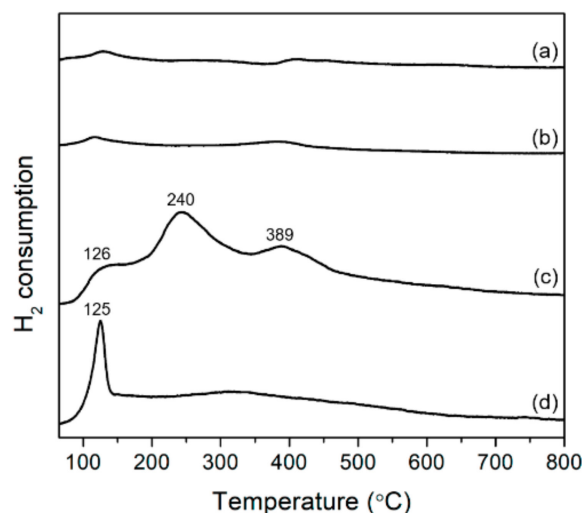


Figure 6. H₂-TPR profiles of supported Pt-Sn catalysts; (a) Pt-Sn/Beta(300), (b) Pt-Sn/Beta(38), (c) Pt-Sn/ θ -Al₂O₃, and (d) Pt-Sn/Q6.

2.2. PDH Catalytic Performance of the Supported Pt-Sn Catalysts

The catalytic activities of the supported Pt-Sn catalysts for PDH were evaluated at the high temperature of 620 °C for acceleration of coke formation and deactivation. Figure 7 shows the time on stream of propane conversion and propylene selectivity over the supported Pt-Sn catalysts. In Table 4, the details are summarized, including the conversion, propylene selectivity, and amount of coke formed. When a blank test was performed in the absence of catalysts, thermal conversion of propane of about 21% was maintained with propylene selectivity of 45%. As a comparison of Pt-Sn catalyst supported over a neutral surface of amorphous silica, the Pt-Sn/Q6 catalyst showed the lowest conversion of 23.6%, which was very similar to that obtained from the blank test. As a feasible candidate for industrial use, the Pt-Sn/ θ -Al₂O₃ catalyst improved the conversion to 60.1% and propylene selectivity to 71.7% at the initial stage of PDH reaction, which can be attributed to high Pt dispersion over the acidic support. This suggests that metal dispersion and metal-support interaction are required to raise the catalytic efficiency of Sn-promoted Pt catalysts. However, rapid deactivation still occurred, and the conversion and propylene selectivity decreased to those of the blank test within a reaction time of 4 h. On the other hand, despite the lower Pt dispersion over Beta zeolites, the Beta zeolite-supported Pt-Sn catalysts exhibited higher conversion than that of the Pt-Sn/ θ -Al₂O₃ catalyst at the initial reaction stage. This result is very similar to that reported by Choi et al. [12], which is that a low concentration of Brønsted acid sites coupled with the presence of strong Lewis acid sites are effective to raise the conversion and propylene selectivity. Nevertheless, the propylene selectivity of the Beta zeolite-supported Pt-Sn catalysts was still lower than that of the Pt-Sn/ θ -Al₂O₃ catalyst at the initial stage. More interestingly, the propylene selectivity over the Beta zeolite-supported Pt-Sn catalysts showed a different reaction trend. Their propylene selectivity increased at 1 h of reaction time and then decreased afterward. After 1 h of reaction time, the Pt-Sn/Beta(300) catalyst outperformed the Pt-Sn/ θ -Al₂O₃ catalyst, showing conversion of 51.4% and propylene selectivity of 72.9%. When the acidity of the Beta zeolites was lowered, this phenomenon was remarkable with slow deactivation.

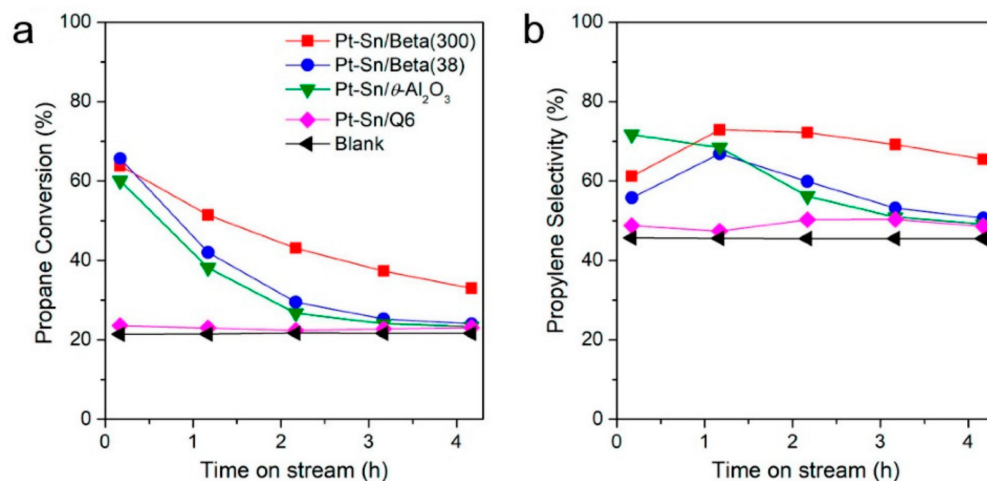


Figure 7. Catalytic performances over different supported Pt-Sn catalysts in propane dehydrogenation (PDH) at 620 °C: (a) propane conversion (%) and (b) propylene selectivity (%).

Table 4. Propane conversion, propylene selectivity, and the amount of coke formed over supported Pt-Sn catalysts during PDH at 620 °C.

Catalyst	Propane Conversion (%)		Propylene Selectivity (%)		Coke (wt%) ^a
	Initial (10 min)	4 h (4 h 10 min)	Initial (10 min)	4 h (4 h 10 min)	
Pt-Sn/Beta(300)	63.8	33.0	61.2	65.5	14.2
Pt-Sn/Beta(38)	65.7	24.0	55.8	50.7	17.5
Pt-Sn/ θ -Al ₂ O ₃	60.1	23.3	71.7	49.2	15.6
Pt-Sn/Q6	23.6	23.1	48.8	48.6	1.3
Blank ^a	21.5	21.7	45.7	45.5	-

^a Blank test was conducted with the same catalytic reaction condition, but in the absence of catalysts.

2.3. Effect of Support on PDH Reaction Mechanism

To decipher the different reaction trend over Beta zeolite-supported Pt-Sn catalysts, the time on streams of selectivity of all the products were compared, as shown in Figure 8. As demonstrated in Scheme 1, propane conversion at high temperature directly undergoes a dehydrogenation step that forms C₃H₆ as a desired product, or a cracking step forms CH₄ and C₂H₄. Then, C₂H₄ can further transform to C₂H₆ via hydrogenation. These light alkanes and alkenes can form larger hydrocarbons through hydrolysis and oligomerization, as well as further alkyl-aromatics through cyclization and dehydrogenation [24,25]. Considering that the blank test produced C₃H₆, C₂H₄, and CH₄ as the main products (Figure 8e), the primary dehydrogenation and cracking steps were competitive at high temperature under our reaction condition. Likewise, Pt-Sn/Q6 followed the similar time on streams of selectivity, so it seems that low dispersion of Pt on Q6 leads it to be catalytically inactive (Figure 8d). Therefore, the improved propylene selectivity over the Pt-Sn/ θ -Al₂O₃ catalyst with high Pt dispersion was achieved by suppressing the cracking step for C₂H₄ and CH₄ (Figure 8c). On the other hand, the Beta zeolite-supported Pt-Sn catalysts led to an increase of not only propylene selectivity but also C₅₊ selectivity at the initial stage (Figure 8a,b). It is well-known that Brønsted acid sites are active sites to catalyze the oligomerization and cyclization steps of alkane aromatization [12,13,24]. Thus, the Pt-Sn/Beta catalysts (containing both Brønsted and Lewis acid sites) could catalyze alkanes/alkenes to alkyl-aromatics, while the Pt-Sn/ θ -Al₂O₃ catalyst (containing only Lewis acid sites) produced very little amount of C₅₊. Considering that these cracked products can cover active sites for PDH, it is likely that the highest propylene selectivity was achieved after a proper period of reaction time (1 h), because the deactivated acid sites could reduce undesirable reactions as the reaction time goes by [9]. Compared to the Pt-Sn/Beta(300), the Pt-Sn/Beta(38)

catalyst with high acidity showed lower propylene selectivity. It is assumed that the Beta zeolite-supported Pt-Sn catalyst with high acidity can induce more side reactions and increase the selectivity of C_{5+} and light gases (C_{1-2}) in comparison to propylene. When the acidity of the Beta zeolite increased, the degree of the deactivation rapidly increased before a better propylene selectivity was achieved. Thus, the Pt-Sn/Beta(300) catalyst with the lowest acidity showed the highest propylene selectivity and slow deactivation.

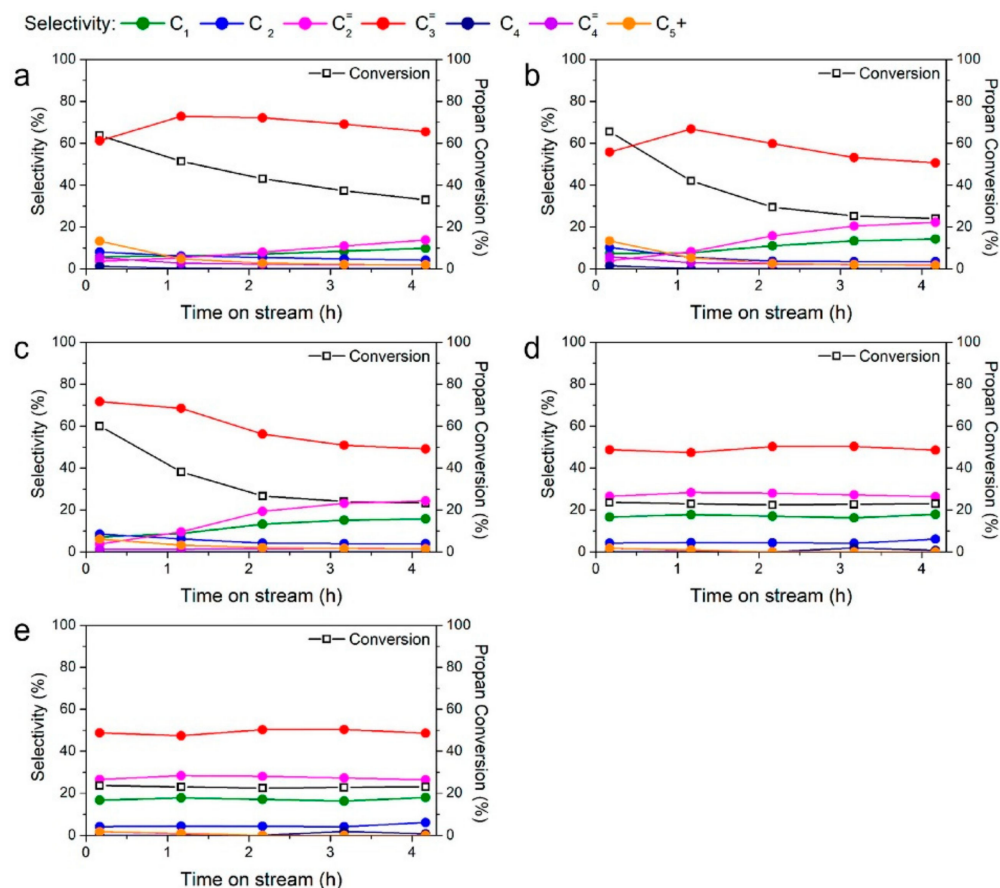
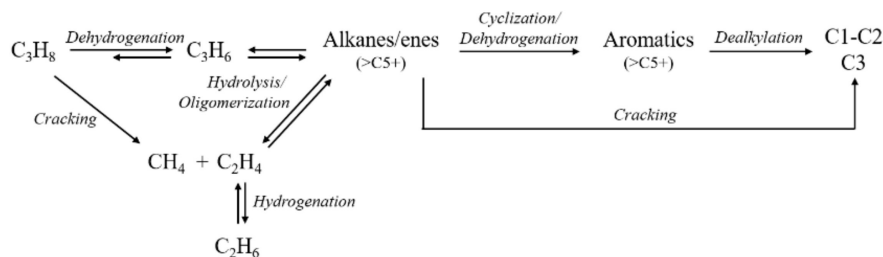


Figure 8. Catalytic performance of PDH over supported Pt-Sn catalysts at 620 °C: (a) Pt-Sn/Beta(300), (b) Pt-Sn/Beta(38), (c) Pt-Sn/ θ -Al₂O₃, (d) Pt-Sn/Q6, and (e) blank test in the absence of catalysts.



Scheme 1. Plausible acid-catalyzed reaction pathways of propane conversion.

To understand slow deactivation observed in the Pt-Sn/Beta(300) catalyst, the amount of coke formed for 4 h of reaction time was estimated by TGA analysis in Table 4. In correlation with the improved conversion, the amount of coke increased in the order of Pt-Sn/Q6 < Pt-Sn/Beta(300) < Pt-Sn/ θ -Al₂O₃ < Pt-Sn/Beta(38). The Pt-Sn/Beta(300) catalyst showed relatively low amount of coke formation despite high propane conversion, but it did not make a significant difference for the explanation of slow deactivation. For a further investigation, the supported Pt-Sn catalysts were collected after the PDH reaction and their Pt-dispersion was reanalyzed by CO chemisorption, as shown in Table 5. While the Pt

dispersion of Pt-Sn/ θ -Al₂O₃ was considerably decreased from 82.8% to 0.8%, those of Pt-Sn/Beta(38) and Pt-Sn/Beta(300) were still preserved as 9.6% and 3.6%, respectively. These results indicate that the Pt surface is less covered by coke in the Beta zeolite-supported Pt-Sn catalysts. To check the blockage of the acid sites by coke, the NH₃-TPD profiles were compared between fresh supported Pt-Sn catalysts and catalysts collected after PDH reaction (Figure S1). All the spent catalysts were pretreated at 300 °C in He stream to avoid the decomposition of coke above 400 °C, as confirmed from TGA profiles (Figure S2). As expected, the Beta zeolite-supported Pt-Sn catalysts showed a considerable decrease in NH₃ desorption peaks in comparison to Pt-Sn/ θ -Al₂O₃ and Pt-Sn/Q6. (Regarding the increased NH₃ desorption at temperature over 400 °C, it seems to indicate the decomposition of the deposited coke, as observed on all the spent catalysts). These results are associated with the reaction mechanism, in which the side reaction is catalyzed by the acid sites in Beta zeolites. Therefore, the Beta zeolite-supported Pt-Sn catalysts form coke near the acid sites on the Beta zeolites, so the coke formed would cover the surface of the Beta zeolites rather than the Pt surface. Meanwhile, the accessible surface area of the Beta zeolite-supported Pt-Sn catalysts is still larger than that of Pt-Sn/ θ -Al₂O₃ according to the surface area and pore volume obtained from the N₂ isotherms shown in Table 5. Although fresh Beta zeolite-supported Pt-Sn catalysts have similar porous properties, the Pt-Sn/Beta(300) catalyst maintained a larger surface area than that of Pt-Sn/Beta(38) after PDH reaction. Conclusively, although the Pt-Sn/Beta(300) catalyst with low acidity showed low Pt dispersion, it formed a relatively lower amount of coke on PDH reaction and maintained a high surface area and active Pt surfaces, resulting in enhanced stability for PDH reaction.

Table 5. Porous properties and Pt-dispersion of supported Pt-Sn catalysts after 4 h of PDH reaction.

Sample	Surface Area (BET) (m ² /g)			Pore Volume (cm ³ /g)			Pt dispersion (%) ^c
	Total ^a	Micropore ^b	Mesopore ^b	Total	Micropore ^b	Mesopore ^b	
Pt-Sn/Beta(300)	270	171	99	0.16	0.07	0.09	3.6
Pt-Sn/Beta(38)	176	98	78	0.13	0.04	0.09	9.6
Pt-Sn/ θ -Al ₂ O ₃	74	-	74	0.21	-	0.21	0.8
Pt-Sn/Q6	342	3	339	0.62	0	0.62	1.7

^a Total surface area was determined by N₂ adsorption and calculated by BET method. ^b Surface area and volume of micropore and mesopore were determined by t-plot method. ^c Pt dispersion was estimated by CO chemisorption.

3. Materials and Methods

3.1. Sample Preparation of Supported Pt-Sn Catalysts

The supported Pt-Sn catalysts were prepared by sequential impregnation method. Each support was prepared by calcining Beta zeolite (Zeolyst international Inc., Conshohocken, PA, USA, CP811C-300 and CP814C, SiO₂:Al₂O₃ = 300 and 38) at 550 °C for 6 h, and Q6 (Fuji Silysia Chemical Ltd., Kasugai, Japan) at 550 °C for 6 h. For the formation of θ -Al₂O₃, boehmite (Sasol North America Inc., Houston, TX, USA, Catapal[®] B) was calcined at 1050 °C for 6 h. For the impregnation of Sn (0.22 wt%), SnCl₂ (Sigma-Aldrich, St. Louis, MO, USA, 99.99%) as precursor was dissolved in the mixture of nitric acid (Duksan, Asan, South Korea, 64–66%) and hydrochloric acid (Samchun, Daejeon, South Korea, 35–37%), and the support was stirred with the mixture for 1.5 h. Then, solvent was removed in the rotary evaporator at 80 °C for 1.5 h, and the product was dried in the oven at 105 °C for 15 h. Afterward, the samples were calcined in the electronic furnace at 700 °C for 3 h. In the same manner, 0.82wt% of Pt was impregnated over Sn loaded samples using H₂PtCl₆•6H₂O (Sigma-Aldrich, 99.95%) as a precursor. After impregnation, the samples were recovered under the same procedure that was employed in the impregnation of Sn, and calcined in the electronic furnace at 600 °C for 3 h. The Beta zeolite-supported Pt-Sn catalysts were denoted as Pt-Sn/Beta(300) and Pt-Sn(38) according to SiO₂/Al₂O₃ ratio of Beta zeolites, and the θ -Al₂O₃ and Q6-supported Pt-Sn catalysts were also denoted as Pt-Sn/ θ -Al₂O₃ and Pt-Sn/Q6, respectively.

3.2. Sample Characterization

N₂ adsorption–desorption measurement was performed using Micromeritics ASAP2020 (Norcross, GA, USA) volumetric analyzer at liquid nitrogen temperature (−196 °C). The samples were degassed under vacuum at 200 °C for 6 h before N₂ adsorption/desorption. The specific surface area was calculated by the Brunauer–Emmett–Teller (BET) method, and the pore volume was measured from the total N₂ adsorption amount.

Temperature programmed desorption (TPD) and temperature programmed reduction (TPR) were carried using BELCAT-B equipped with a thermal conductivity detector (TCD):

(1) For NH₃-TPD, the sample was pretreated by heating at 10 °C/min in a 5% H₂/Ar up to 620 °C and being kept for 1 h. After pretreatment, it was cooled to 100 °C for 0.5 h in the He stream, and then saturated by ammonia for 0.5 h in 30% NH₃/He. Prior to analysis, the sample was purged for 1.5 h in He stream to eliminate physisorbed ammonia. The temperature increased up to 600 °C at 10 °C/min under He stream and the desorption profiles of ammonia were detected by TCD. For the spent samples, the NH₃-TPD profiles were obtained with the same procedure, except that the pretreatment was conducted by heating at 10 °C/min in He stream up to 300 °C and being kept for 1 h.

(2) For H₂-TPR, the sample was pretreated by heating at 10 °C/min in a He flow up to 150 °C and being kept for 2 h. Then, it was cooled down to 40 °C, and the He flow was converted to a 5% H₂/Ar flow and stabilized for 2 h. When the TCD signal was stabilized, temperature and the hydrogen consumption profiles were recorded by heating the sample up to 1000 °C at a constant rate of 10 °C/min.

Fourier transformation infrared (FT-IR) spectra of adsorbed pyridine were measured by FT-IR spectrometer (Thermo SCIENTIFIC, Waltham, MA, USA, Nico-let6700) equipped with thermal detector. A sample was pressed to make a thin wafer (ca. 14 mg) without binding agents. In an IR cell, the thin wafer was pretreated at 300 °C for 2 h and cooled down to 50 °C. The spectrum of the pretreated thin wafer was recorded as reference. Pyridine was adsorbed in the sample wafer in a He flow saturated by pyridine for 5 min, and the physisorbed pyridine was removed under a He flow at 150 °C for 5 h. Then, the FT-IR spectrum of the pyridine-adsorbed sample wafer was recorded. For a study of pyridine adsorbed on Brønsted and Lewis acid sites, the FT-IR spectrum was refined by subtracting the FT-IR spectrum of “the pretreated sample wafer” from that of “the pyridine-adsorbed”.

Transmission electron microscopy (TEM) images were obtained by a FEI-Talos F200S field emission gun transmission and scanning transmission electron microscope (FEG-S/TEM) operated at 200 kV.

CO chemisorption was carried out for the measurement of Pt dispersion of the prepared catalysts using Micromeritics ASAP2020C volumetric analyzer. For this, 0.1 g of each sample was treated under a He flow at 110 °C for 0.5 h. Subsequently, the sample was heated up to 350 °C under pure H₂ flow and hold up for 3 h. After the sample reduction, a purge was performed under He flow at identical temperature for 2 h. Then, the sample was cooled down to 35 °C, and purged under He flow for 2 h. After the pretreatment and the reduction, the sample was streamed in CO as adsorbate for total adsorption. Afterward, the sample was evacuated to remove physically adsorbed CO and restreamed in CO for physical adsorption. The amount of chemisorbed CO was calculated from the difference of between two quantities of adsorbed CO.

X-ray diffraction (XRD) patterns of the samples were obtained using a diffractometer (Rigaku, Tokyo, Japan, Ultima IV) with monochromatic Cu K α radiation ($\lambda = 1.5418 \text{ \AA}$) of graphite monochromator at 40 kV and 40 mA.

Thermal gravimetric analysis (TGA) was conducted using a TA-60WS thermogravimetric analyzer (Simadzu, Kyoto, Japan) to estimate the amount of coke formed in catalysts after catalytic performance test. The spent catalyst was washed twice with acetone and collected by centrifugation. Then, the collected sample was pretreated by heating at 10 °C/min in a N₂ flow up to 200 °C and stabilizing for 0.5 h. It was heated from 50 °C to 1000 °C at

10 °C/min in an air atmosphere and the TGA curve was obtained from the change of the sample weight.

3.3. Catalytic Performance Test

Catalytic performance of propane dehydrogenation was tested in continuous fixed-bed reaction system with 0.5 g of the catalyst into quartz tube reactor. The catalyst was reduced at 620 °C for 2 h in 50% H₂/N₂ flow (100 SCCM). Then, the reaction mixture composed of N₂/C₃H₈ without H₂ (N₂/C₃H₈ mol ratio = 1:10, weight hourly space velocity (WHSV) = 6 h⁻¹) was fed to the reactor under atmospheric pressure at high temperature of 620 °C for acceleration of coke formation. Product gas was analyzed using on-line gas chromatography Younglin YL 6100GC equipped with capillary column (Agilent technologies, Santa Clara, CA, USA, GS-GASPRO, 0.320 mm, 50 m). The signal was detected by Flame Ionization Detector (FID) and TCD.

4. Conclusions

In summary, this work demonstrates that the use of Beta zeolite as a support can alter the physicochemical properties and catalytic properties of supported Pt-Sn catalysts for PDH reaction compared with θ -Al₂O₃ and Q6. On the surface of Beta zeolites, Lewis acid sites can enhance the reaction conversion by increasing the metal dispersion, and Brønsted acid sites can act as active sites for cracking, oligomerization, and aromatization. Thus, the Beta zeolite-supported Pt-Sn catalysts achieved enhanced propane conversion, but the formation of C₅₊ and light gases (C₁₋₂) was observed due to Brønsted acid sites at the initial stage. After a particular reaction time, these cracked products covered the acid sites, and the side reaction was suppressed, resulting in an increased propylene selectivity before catalyst deactivation. From the comparison between Beta zeolites-supported Pt-Sn catalysts with SiO₂/Al₂O₃ ratio of 38 and 300, the Pt-Sn/Beta(300) catalyst exhibited the best PDH catalytic activity in spite of lower Pt dispersion. According to the characterization and PDH catalytic behavior of Beta zeolite-supported Pt-Sn catalysts, zeolite-supported Pt-Sn catalysts can be the advantageous catalyst candidate to enhancing the selectivity and stability for PDH reaction. Large surface area enables high Pt dispersion as active catalytic sites and proper acidity is crucial to reduce coke formation by altering the reaction mechanism with Brønsted acid sites participating in oligomerization and cyclization steps of alkane aromatization. Overall, this work can provide a better understanding of zeolite-supported Pt-Sn catalysts to improve PDH catalytic activity with high selectivity and low coke formation.

Supplementary Materials: The following are available online at <https://www.mdpi.com/2073-4344/11/1/25/s1>, Figure S1: NH₃-TPD profiles of supported Pt-Sn catalysts collected after propane conversion, Figure S2: TGA profiles of Pt-Sn supported catalysts collected after propane conversion.

Author Contributions: Conceptualization, S.-U.L. and J.-R.K.; methodology, S.-U.L. and J.-R.K.; validation, S.-U.L., Y.-J.L., S.-J.K., S.-Y.J., and J.-R.K.; formal analysis, S.-U.L., Y.-J.L., and S.-J.K.; investigation, S.-U.L., Y.-J.L., S.-J.K., S.-Y.J., and J.-R.K.; data curation, S.-U.L. and Y.-J.L.; writing—original draft preparation, S.-U.L.; writing—review and editing, S.-U.L. and J.-R.K.; visualization, S.-U.L. and Y.-J.L.; supervision, J.-R.K.; project administration, J.-R.K.; funding acquisition, S.-Y.J. and J.-R.K. All authors have read and agreed to the published version of the manuscript.

Funding: This work was supported by the industry core technology development project of the Ministry of Trade, Industry and Energy (project no.: 100052754) and the core KRICT project (grant no.: SI2011-30).

Institutional Review Board Statement: Not applicable.

Informed Consent Statement: Not applicable.

Data Availability Statement: The data presented in this study are available on request from the corresponding author.

Conflicts of Interest: The authors declare no conflict of interest. The funding sponsors had no role in the design of the study; in the collection, analyses, or interpretation of data; in the writing of the manuscript; and in the decision to publish the results.

References

1. Li, J.; Qi, Y.; Zhang, D.; Liu, Z. Propylene production by co-reaction of ethylene and chloromethane over SAPO-34. In *Studies in Surface Science and Catalysis*; Xu, R., Gao, Z., Chen, J., Yan, W., Eds.; Elsevier: Amsterdam, The Netherlands, 2007; pp. 1578–1582.
2. Ahmed, M.H.M.; Masuda, T.; Muraza, O. The role of acidity, side pocket, and steam on maximizing propylene yield from light naphtha cracking over one-dimensional zeolites: Case studies of EU-1 and disordered ZSM-48. *Fuel* **2019**, *258*, 116034. [[CrossRef](#)]
3. Mackenzie, W. *Propylene Global Supply Demand Analytics Service*; Wood Mackenzie: Edinburgh, UK, 2018.
4. Alotibi, M.F.; Alotibi, M.F.; Alshammari, B.A.; Alotaibi, M.H.; Alotaibi, F.M.; Alshihri, S.; Navarro, R.M.; Fierro, J.L.G. ZSM-5 Zeolite Based Additive in FCC Process: A Review on Modifications for Improving Propylene Production. *Catal. Surv. Asia* **2020**, *24*, 1–10. [[CrossRef](#)]
5. Rodríguez, D.; Sánchez, J.; Arteaga, G. Effect of tin and potassium addition on the nature of platinum supported on silica. *J. Mol. Catal. A Chem.* **2005**, *228*, 309–317. [[CrossRef](#)]
6. Dittrich, C.J. The role of heat transfer on the feasibility of a packed-bed membrane reactor for propane dehydrogenation. *Chem. Eng. Trans.* **2020**, *381*, 122492–122505. [[CrossRef](#)]
7. Zhu, X.; Liu, S.; Song, Y.; Xu, L. Catalytic cracking of C4 alkenes to propene and ethene: Influences of zeolites pore structures and Si/Al₂ ratios. *Appl. Catal. A* **2005**, *288*, 134–142. [[CrossRef](#)]
8. Wang, Y.; Tian, Z.-P.W.; Gao, L.; Wang, Z.; Yuan, Z.-Y. Framework-confined Sn in Si-beta stabilizing ultra-small Pt nanoclusters as direct propane dehydrogenation catalysts with high selectivity and stability. *Catal. Sci. Technol.* **2019**, *9*, 6993–7002. [[CrossRef](#)]
9. Nawaz, Z.; Xiaoping, T.; Fei, W. Influence of operating conditions, Si/Al ratio and doping of zinc on Pt-Sn/ZSM-5 catalyst for propane dehydrogenation to propene. *Korean J. Chem. Eng.* **2009**, *26*, 1528–1532. [[CrossRef](#)]
10. Zhang, Y.; Zhou, Y.; Qiu, A.; Wang, Y.; Xu, Y.; Wu, P. Propane dehydrogenation on PtSn/ZSM-5 catalyst: Effect of tin as a promoter. *Catal. Commun.* **2006**, *7*, 860–866. [[CrossRef](#)]
11. Al-majnouni, K.A.; Yun, J.H.; Lobo, R.F. High-Temperature Produced Catalytic Sites Selective for n-Alkane Dehydrogenation in Acid Zeolites: The Case of HZSM-5. *ChemCatChem* **2011**, *3*, 1333–1341. [[CrossRef](#)]
12. Choi, S.-W.; Kim, W.-G.; So, J.-S.; Moore, J.S.; Liu, Y.; Dixit, R.S.; Pendergast, J.G.; Sievers, C.; Sholl, D.S.; Nair, S.; et al. Propane dehydrogenation catalyzed by gallosilicate MFI zeolites with perturbed acidity. *J. Catal.* **2017**, *345*, 113–123. [[CrossRef](#)]
13. De Cola, P.L.; Gläser, R.; Weitkamp, J. Non-oxidative propane dehydrogenation over Pt-Zn-containing zeolites. *Appl. Catal. A* **2006**, *306*, 85–97. [[CrossRef](#)]
14. Liu, L.; Lopez-Haro, M.; Lopes, C.W.; Rojas-Buzo, S.; Concepcion, P.; Manzorro, R.; Simonelli, L.; Sattler, A.; Serna, P.; Calvino, J.J.; et al. Structural modulation and direct measurement of subnanometric bimetallic PtSn clusters confined in zeolites. *Nat. Catal.* **2020**, *3*, 628–638. [[CrossRef](#)]
15. Xu, Z.; Yue, Y.; Bao, X.; Xie, Z.; Zhu, H. Propane Dehydrogenation over Pt Clusters Localized at the Sn Single-Site in Zeolite Framework. *ACS Catal.* **2020**, *10*, 818–828. [[CrossRef](#)]
16. Sun, L.; Chai, Y.; Dai, W.; Wu, G.; Guan, N.; Li, L. Oxidative dehydrogenation of propane over Pt-Sn/Si-beta catalysts: Key role of Pt-Sn interaction. *Catal. Sci. Technol.* **2018**, *8*, 3044–3051. [[CrossRef](#)]
17. Prakash, N.; Lee, M.-H.; Yoon, S.; Jung, K.-D. Role of acid solvent to prepare highly active PtSn/ θ -Al₂O₃ catalysts in dehydrogenation of propane to propylene. *Catal. Today* **2017**, *293–294*, 33–41. [[CrossRef](#)]
18. Lucas, A.D.; Ramos, M.J.; Dorado, F.; Sánchez, P.; Valverde, J.L. Influence of the Si/Al ratio in the hydroisomerization of n-octane over platinum and palladium beta zeolite-based catalysts with or without binder. *Appl. Catal. A* **2005**, *289*, 205–213. [[CrossRef](#)]
19. Smirnova, M.Y.; Kikhtyanin, O.V.; Smirnov, M.Y.; Kalinkin, A.V.; Titkov, A.I.; Ayupov, A.B.; Ermakov, D.Y. Effect of calcination temperature on the properties of Pt/SAPO-31 catalyst in one-stage transformation of sunflower oil to green diesel. *Appl. Catal. A* **2015**, *505*, 524–531. [[CrossRef](#)]
20. Radivojević, D.; Seshan, K.; Lefferts, L. Preparation of well-dispersed Pt/SiO₂ catalysts using low-temperature treatments. *Appl. Catal. A* **2006**, *301*, 51–58. [[CrossRef](#)]
21. Zhu, H.; Anjum, D.H.; Wang, Q.; Abou-Hamad, E.; Emsley, L.; Dong, H.; Laveille, P.; Li, L.; Samal, A.K.; Basset, J.-M. Sn surface-enriched Pt-Sn bimetallic nanoparticles as a selective and stable catalyst for propane dehydrogenation. *J. Catal.* **2014**, *320*, 52–62. [[CrossRef](#)]
22. Lieske, H.; Lietz, G.; Spindler, H.; Völter, J. Reactions of platinum in oxygen- and hydrogen-treated Pt/ γ -Al₂O₃ catalysts: I Temperature-programmed reduction, adsorption, and redispersion of platinum. *J. Catal.* **1983**, *81*, 8–16. [[CrossRef](#)]
23. Xu, G.; Zhang, J.; Wang, S.; Zhao, Y.; Ma, X. A well fabricated PtSn/SiO₂ catalyst with enhanced synergy between Pt and Sn for acetic acid hydrogenation to ethanol. *RSC Adv.* **2016**, *6*, 51005–51013. [[CrossRef](#)]
24. Yun, J.H.; Lobo, R.F. Radical Cation Intermediates in Propane Dehydrogenation and Propene Hydrogenation over H-[Fe] Zeolites. *J. Phys. Chem. C* **2014**, *118*, 27292–27300. [[CrossRef](#)]
25. Zhu, X.; Lobban, L.L.; Mallinson, R.G.; Resasco, D.E. Tailoring the mesopore structure of HZSM-5 to control product distribution in the conversion of propanal. *J. Catal.* **2010**, *271*, 88–98. [[CrossRef](#)]